Electronic Supplementary Information

Electrolyte Design Implications of Ion-Pairing in Low-Temperature Li Metal Batteries

John Holoubek[a], Kangwoon Kim[b], Yijie Yin[b], Zhaohui Wu[c], Haodong Liu[a], Mingqian Li[c], Amanda Chen[c], Guorui Cai[a], Tod A. Pascal[a,b,c,d], Ping Liu[a,b,c,d,*], Zheng Chen[a,b,c,d,*]

[a]*Department of NanoEngineering, University of California, San Diego, La Jolla, CA 92093, USA*

[b]*Program of Materials Science, University of California, San Diego, La Jolla, CA 92093, USA*

[c]*Program of Chemical Engineering, University of California, San Diego, La Jolla, CA 92093, USA*

[d]*Sustainable Power and Energy Center, University of California, San Diego, La Jolla, CA 92093, USA*

Experimental Methods

Materials. Anhydrous 1,2-dimethoxyethane (DME) were purchased from Millipore-Sigma and used as received. Bis(2,2,2-trifuloroethyl) ether (BTFE) was purchased from Synquest, and dried with activated molecular sieves for at least 24 hrs before use. Lithium bis(fluorosulfonyl)imide (LiFSI) was obtained from Kelude and used as received. The electrolytes were prepared dissolving predetermined amounts of LiFSI salt into the solvents of interested and stirred. $LiNi_{0.8}Co_{0.2}Mn_{0.2}O_2$ (NMC 811) was purchased from Targray. The NMC 811 electrodes were prepared by mixing the NMC 811 powder, Super-P and PVDF (KYNAR 2800) in a ratio of 96:2:2 in N-methyl pyrrolidinone (NMP, Sigma) solvent, cast on Al foil (MTI) and dried in a vacuum oven at 120 °C overnight, and calendared in a mechanical roller.

For electrochemical tests CR-2032 or CR-2016 type coin cells were assembled with prepared cathodes and anode separated by a 25 μm Celgard membrane soaked with 75 μL of electrolyte. For Li metal performance tests, 250 μm Li metal chips were purchased from Xiamen TOB New Energy Technology Co. LTD. and paired with Cu foil for Li||Cu cells, or an identical Li chip in Li||Li cells. Both Li||Cu and Li||Li cells employed CR-2032 cells. Linear scan voltammetry (LSV) stability tests were conducted with 250 μm Li and a blocking working electrode made of Al foil. 2x Li||NMC811 full cells were assembled with a 2.1 ± 0.1 mAh cm^{-2} (10.5 ± 0.5 mg cm^{-2}) NMC 811 electrode and a Li counter electrode that was electroplated beforehand in a separate Li||Cu cell utilizing the electrolyte of interest at room-temperature. The efficiency for the electroplated anode was determined to be 90 and 96 % for 1 M LiFSI DME and 1 M LiFSI BTFE/DME (5:1), respectively in separate tests and accounted for in the anode preparation. The full cells were finally assembled in CR-2016 coin cells with aluminum foil protection on the cathode side of the coin cell case, which has been shown to reduce oxidative reactivity of ether electrolytes.[1]

Characterization. The morphology of the deposited Li metal at various temperatures was characterized using a FEI Quanta 250 SEM. The samples were obtained from coin cells and

washed with DME before analysis. All prepared samples were placed in a heat-sealed bag inside the glovebox before they were transferred to the SEM. The ionic conductivity of the electrolyte was measured by a customized two-electrode coin cell, in which the two stainless-steel electrodes are spaced symmetrically between a polytetrafluoroethylene washer with a thickness of 0.027 inches. A glass-fiber separator soaked with electrolyte was housed on the inside of the washer, constraining its surface area to a known value. The electrolyte conductivity values were then obtained with electrochemical impedance spectroscopy (EIS) using the following equation: $\sigma = \frac{L}{A*R}$, where R is the measured ionic resistance and A and L are the area of and space between the electrodes, respectively. The data points from 40 ^{o}C to -60 ^{o}C were measured in an ESPEC BTX-475 temperature chamber to maintain the cell at a set temperature for 1 hour intervals before each measurement. Raman spectroscopy was conducted on a Renishaw *inVia* upright microscope with an x-y mapping stage, where the electrolyte of interest was pipetted onto a covered concave microscope slide before measurement. A 532 nm laser source was applied with 3 exposure sweeps when collecting each spectrum.

XPS (Kratos Analytical, Kratos AXIS Supra) was carried out using Al anode source at 15 kV and all the peaks were fitted based on the reference C-C bond at 284.6 eV. All XPS measurements were collected with a 300 mm × 700 mm spot size during acquisition. Survey scans were collected with a 1.0 eV step size, and were followed by high resolution scans with a step size of 0.05 eV for C 1s, O 1s, F 1s, and S2p regions. When applied, etching was carried out at a 5 nm min^{-1} rate based on Si. Li metal samples applied to etching were cycled 10 times at room temperature in Li||Cu cells at 1 mA cm^{-2}, whereas Li metal samples applied to temperature dependent analysis were deposited at 4 mAh cm^{-2} in Li||Cu cells without cycling. NMC 811 cathodes were cycled 10 times at room temperature at C/3 rate before analysis. All prepared samples were obtained from coin cells and washed with DME and then placed in a heat-sealed bag inside the glovebox before they were transferred to the XPS.

Electrochemical Testing. All electrochemical data provided in this work were produced by CR-2032 and CR-2016 type coin cells assembled in an Ar filled glovebox kept at < 0.5 ppm O_2 and < 0.1 ppm H_2O. All low temperature data points were obtained from these cells inside SolidCold C4-76A and SolidCold C-186A ultra-low chest freezers for -40 ^{o}C and -60 ^{o}C tests, respectively. Cells were rested for at least 2 hr at low temperature to achieve equilibration. Low temperature galvanostatic testing was done on an Arbin LBT-10V5A system, while room temperature galvanostatic testing was done on a Neware BTS 4000 system. All potentiostatic tests were carried out on a Biologic VSP-300 potentiostat.

The transference numbers of the electrolytes were determined via a commonly applied potentiostatic polarization technique on a Biologic VSP-300 potentiostat in which 10 mV was applied for 2 hr to a Li||Li cell with 5 Celgard separators to obtain the initial current I_0, where the cation concentration is uniform and the current corresponds to both the cations and anions, and the steady state current I_{ss}, which is only attributed to the cations. EIS was applied before and after the polarization in order to obtain the cell impedance, where the transference number was then calculated using the following equation:

$$t_+ = \frac{I_{SS}(\Delta V - I_0 R_0)}{I_0(\Delta V - I_{SS} R_{SS})}$$

where ΔV is the applied bias, R_0 is the initial cell impedance, and R_{SS} is the steady state cell impedance.

Three-electrode cells were assembled by including an additional wire with a small amount of Li metal attached between each electrode in Li||NMC 811 coin cells. 2 separators were used to isolate the reference electrode, and sealed in the same fashion as 2-electrode cells. Floating voltage measurements were conducted in Li||NMC 811 cells according to previous literature.[2] After charging to 4.3 V at C/10, 4.3, 4.4, 4.5, and 4.6 V holds were sequentially imposed for 10 hrs each.

Li metal coulombic efficiency (CE) measurements were carried out on Li||Cu cells using the accurate CE determination method.[3] Prior to the test, a condition cycle was carried out on all the cells, where 4 mAh cm^{-2} of Li was deposited onto the Cu foil at 0.5 mA cm^{-2}, and then fully stripped to 1 V to form the SEI before CE testing. During testing 4 mAh cm^{-2} was first deposited followed by 10 cycles of 1 mAh cm^{-2} plating and stripping before finally stripping all Li to 1 V. The CE was calculated by dividing the total stripped capacity by the total plated capacity. The morphological Li studies at various temperatures were conducted on Cu working electrodes plated with 5 mAh cm^{-2} at 0.5 mA cm^{-2} in Li||Cu cells at room temperature as well as -40 ^{o}C. The oxidative stability of the electrolytes was determined via LSV of a Li||Al cell at 1 mV s^{-1}.

Li||NMC 811 cells were assembled and subjected to galvanostatic cycling at room temperature and -40 ^{o}C and -60 ^{o}C inside the respective chest freezers after resting for 2 hours to achieve temperature equilibration. For the low temperature tests, a room temperature charge was first carried out at C/10 and transferred to a chamber set at the temperature of interest for cycling. Room temperature cycling consisted of 2 conditioning cycles at C/10 followed by C/3 indefinitely for both charge and discharge. Low temperature cycling was conducted at C/10 for charge and C/5 for discharge. The specific capacity basis for C rate determination was 200 mAh g^{-1} with respect to the cathode.

MD Simulations. Molecular Dynamics (MD) simulations were performed in LAMMPS using the OPLS-AA forcefield[4] with the FSI molecules description from Gaouveia et al.[5] For electrolyte structure determination, simulation boxes containing ~500 total molecules were constructed using various ratios of each component as dictated by the stoichiometry of each system (Table S1). In all cases the charges of the Li^{+} and FSI^{-} molecules were scaled to the high-frequency dielectric properties of the solvents present in the system according to the method proposed by Park *et al*.[6] These scaling values were 0.73, 0.75, 0.76, 0.76, and 0.76 for 1 M LiFSI in BTFE/DME 0:1, 1:1, 3:1, 5:1, and 7:1, respectively.

For each system, an initial energy minimization at 0 K (energy and force tolerances of 10^{-4}) was performed to obtain the ground-state structure. After this, the system was slowly heated from 0 K to room temperature at constant volume over 0.01 ns using a Langevin thermostat, with a damping parameter of 100 ps. The system was then subjected to 5 cycles of quench-annealing dynamics in order to eliminate the persistence of any meta-stable states, where the temperature was slowly cycled between 298 K and 894 with a ramp period 0.025 ns followed by 0.1 ns of dynamics at either temperature extreme. All 5 anneal cycles thus take 1.25 ns total. After annealing, the system was equilibrated in the constant temperature (298 K), constant pressure (1bar) (NpT ensemble) for 1.5 ns. We resolved stresses in the system isotropically using the Andersen barostat (pressure relaxation constant of 1 ps). We used the Shinoda et al.[7] equations of motion which combine the hydrostatic equations of Martyna et al.[8] with the strain energy proposed by Parrinello and Rahman[9]. The time integration schemes closely follow the time-reversible measure-preserving Verlet integrators derived by Tuckerman et al.[10] Finally, we performed 25 ns of constant volume, constant temperature (NVT) production dynamics at 298 K.

Radial distribution functions were obtained using the Visual Molecular Dynamics (VMD) software. Simulated transference numbers were calculated by extracting the diffusion coefficients

of Li^+ and FSI^- from the latter half of the production dynamics trajectory with VMD, and applying them in the following formula:

$$t_+ = \frac{D_{Li+}}{(D_{Li+} + D_{FSI-})}$$

Pictures of the various solvation shells, sampled from the simulation trajectory, where also obtained using VMD. Solvation speciation was determined via a series of in-house codes. First, each Li^+ and every molecule within 3 Å were sampled every 0.1 ns via a Tcl script implemented through VMD. This script generated between 10,750 and 12,500 snapshots depending on the number of Li^+ in each simulation (see above). Next, the number of DME, FSI^-, and BTFE in each snapshot were tallied using Python and aggregated into a distribution of X-Y-Z shells corresponding to $[Li(DME)_x(FSI)_y(BTFE)_z]^{y+1}$ complexes.

Quantum Chemistry Calculations. Quantum chemistry simulations were performed using the Q-Chem 5.1 quantum chemistry package[11]. Simulations involved a geometry optimization step at the B3LYP//6-31+G(d,p) level of theory followed by single point energy and harmonic vibrational analysis at the B3LYP//6-311++G** level of theory. Removal energies of various solvation species of the $[Li(DME)_x(FSI)_y]^{y+1}$ complexes were calculated as:

$$\Delta E = E_{Li^+(DME)_x(FSI^-)_y} - (E_{Li^+(DME)_{x-1}(FSI^-)_y} + E_{DME}) \text{ or}$$

$$\Delta E = E_{Li^+(DME)_x(FSI^-)_y} - (E_{Li^+(DME)_x(FSI^-)_{y-1}} + E_{FSI^-})$$

In all cases, an implicit solvent was enforced using the polarizable continuum with 194 Lebedev grid points using Bondi radii. The enforced optical and static dielectric constants were 1.902 and 7.2, respectively, which corresponds to DME.

Cell Level Energy Density Calculations. The cell level energy densities for this work were calculated via the 18650-cylinder cell model proposed by Betz *et al* that we adapted for pouch-type configurations.[12] Unless specified otherwise, the materials metrics (e.g., current collector thickness/density) from this work were used. It was assumed that a 30 % cathode porosity, a 0 % Li porosity, and an electrolyte loading of 3 g Ah^{-1} was achievable and were used in the calculation. The cathode and anode dimensions were assumed to be 4.4 x 5.7 and 4.5 x 5.8, respectively. The pouch cell film parameters and positive/negative tab masses were measured experimentally from products purchased from MTI. An N/P capacity ratio of 2 was assumed to match the loading demonstrated in this work. For each cathode loading, the number of cathode and anode layers was adjusted manually to achieve a projected total capacity of 5 Ah. The number of double-sided anodes, double-sided cathodes, and single-sided cathodes were taken as x, x-1, and 2, respectively. Enough pouch film to provide 20% extra stack thickness was assumed, which is generally required to provide enough area for sealing. For projections at each temperature, the specific capacity and average discharge voltage of the coin cells employing both electrolytes of interest were used (Table S2). However, it was assumed that the loadings of each component were maintained based on the room-temperature performance so as to not inflate the low temperature energy densities (e.g., 3 g Ah^{-1} of electrolyte was based off of the specific capacity of the cathode at room temperature).

Table S1. Number of electrolyte components for classical MD simulations.

Electrolyte System	**# LiFSI Molecules in Box**	**# DME Molecules in Box**	**# BTFE Molecules in Box**
1 M LiFSI DME	43	414	0
1 M LiFSI BTFE/DME (1:1)	47	226	181
1 M LiFSI BTFE/DME (3:1)	49	118	283
1 M LiFSI BTFE/DME (5:1)	50	80	321
1 M LiFSI BTFE/DME (7:1)	50	60	337

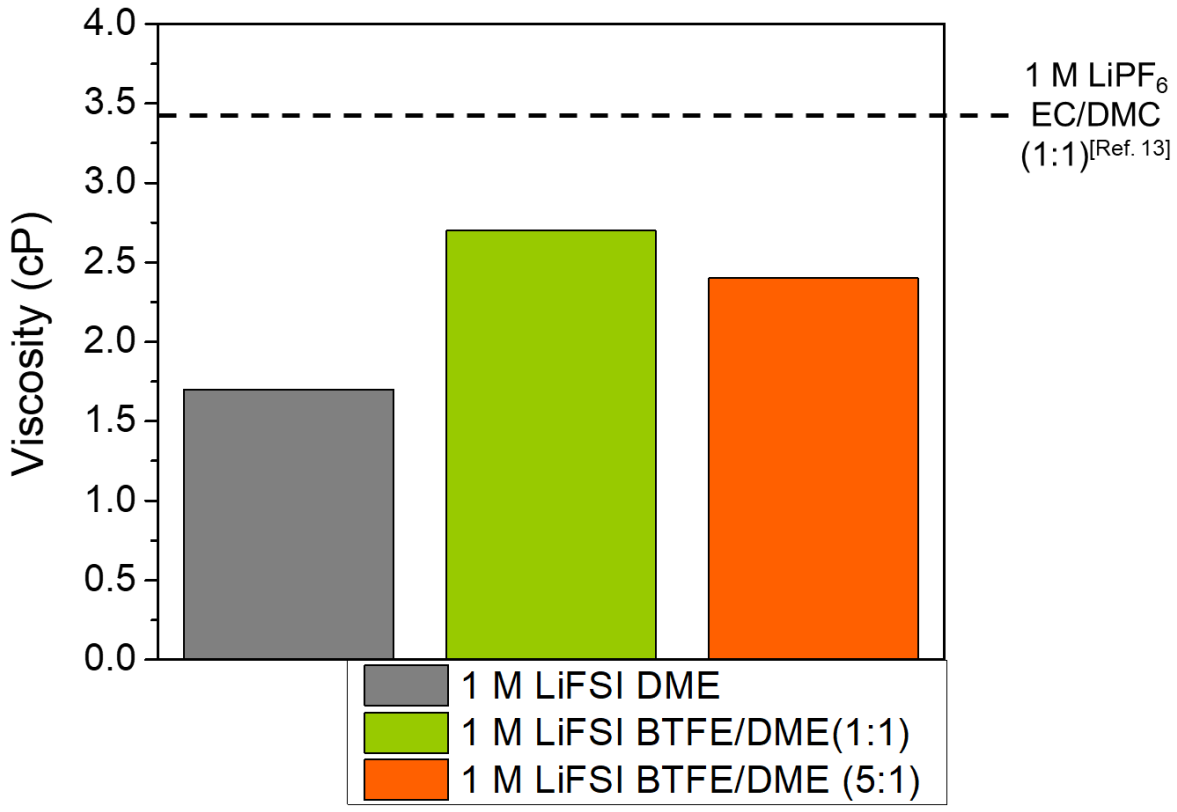

Figure S1. Measured viscosity of selected electrolytes.

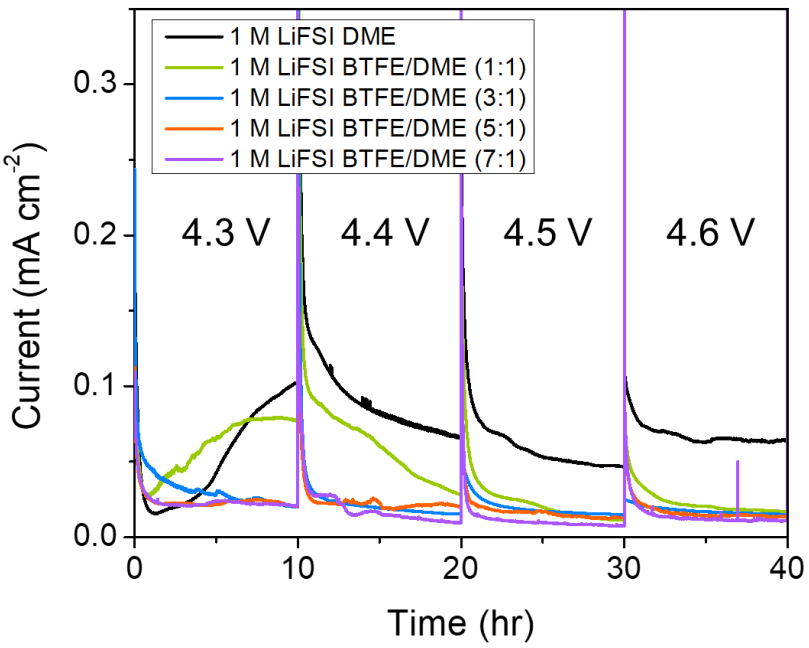

Figure S2. Floating voltage profiles of NMC 811 cathodes in electrolytes of interest. The noise observed at increased voltage is attributed to corrosion events between the current collector and the electrolyte.

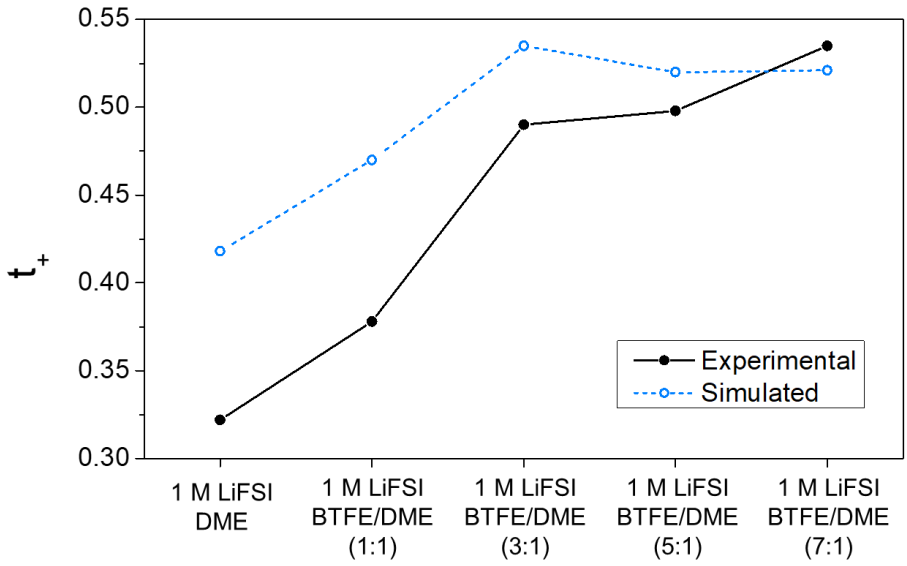

Figure S3. Measured and simulated Li^+ transference numbers of electrolytes of interest.

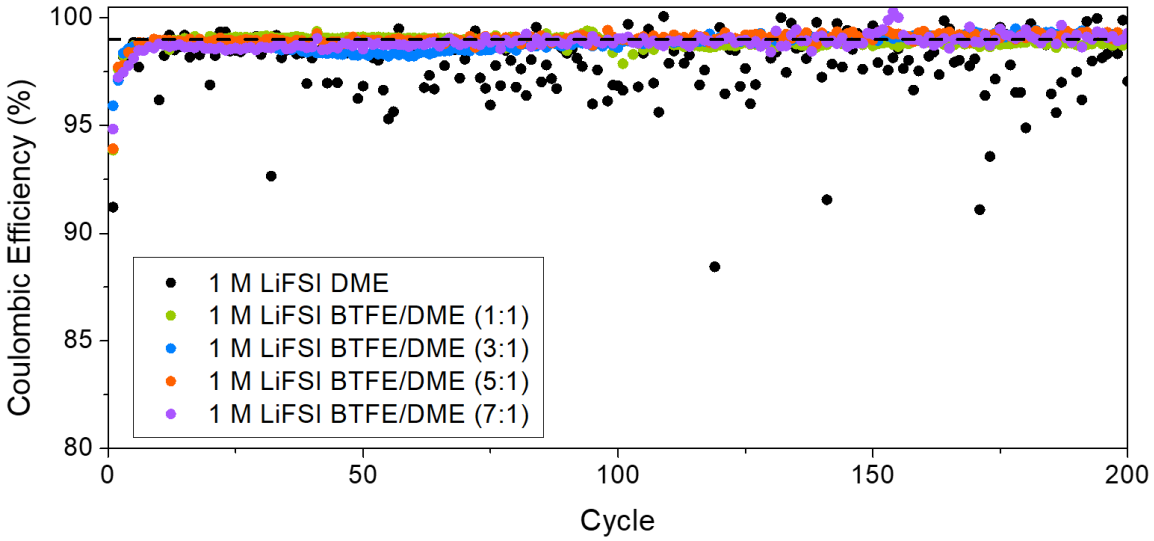

Figure S4. Extended plating/stripping efficiency of Li||Cu cells in the electrolyte of interest at 0.5 mA cm^{-2} and 1 mAh cm^{-2}. The dotted line is set at 99 % CE.

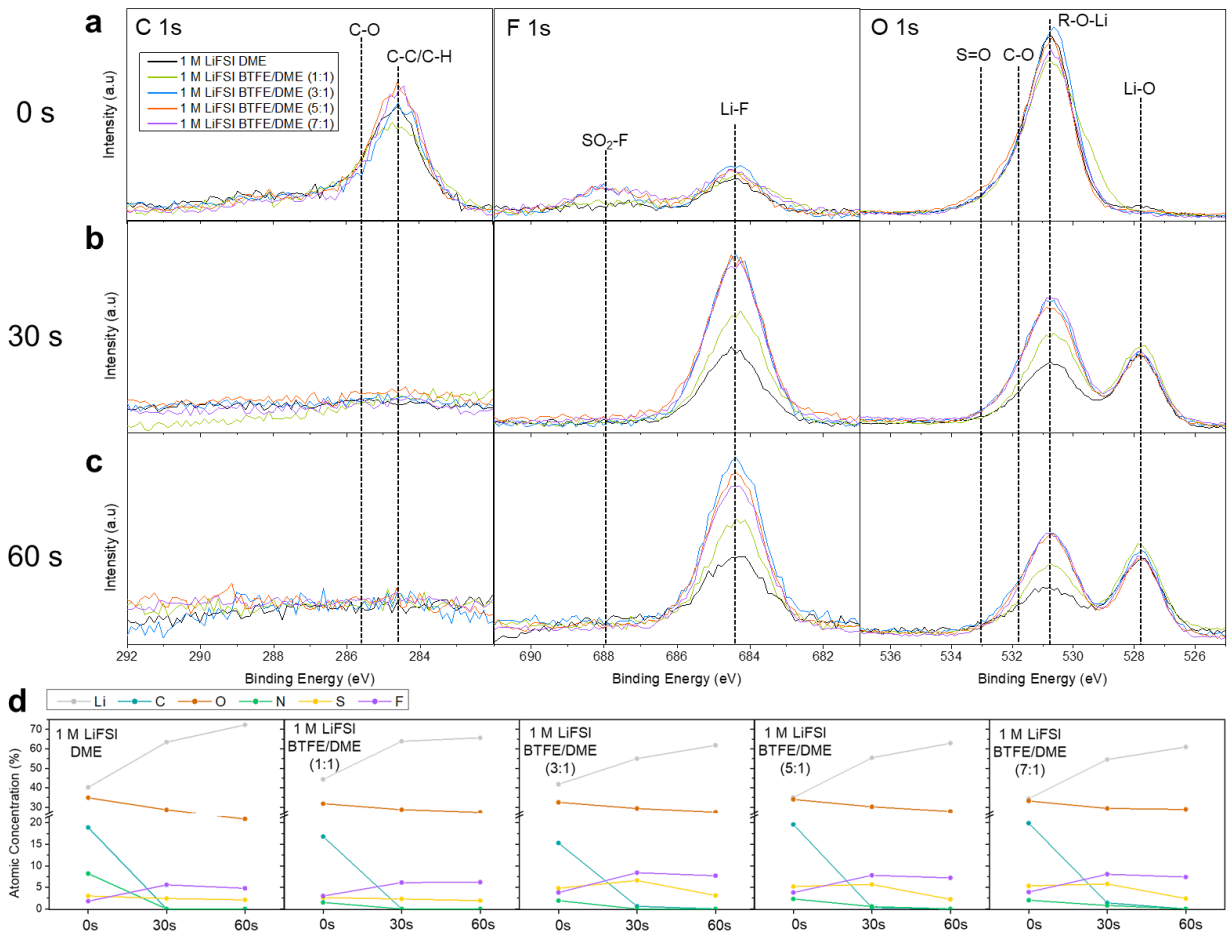

Figure S5. XPS spectra of Li metal after 10 cycles in electrolytes of interest. **a)** C 1s, F 1s, and O 1s surface spectra, **b)** C 1s, F 1s, and O 1s surface spectra after 30 s of etching **c)** C 1s, F 1s, and O 1s surface spectra after 60 s of etching. **d)** Elemental composition of electrolytes of interest with increasing etch time.

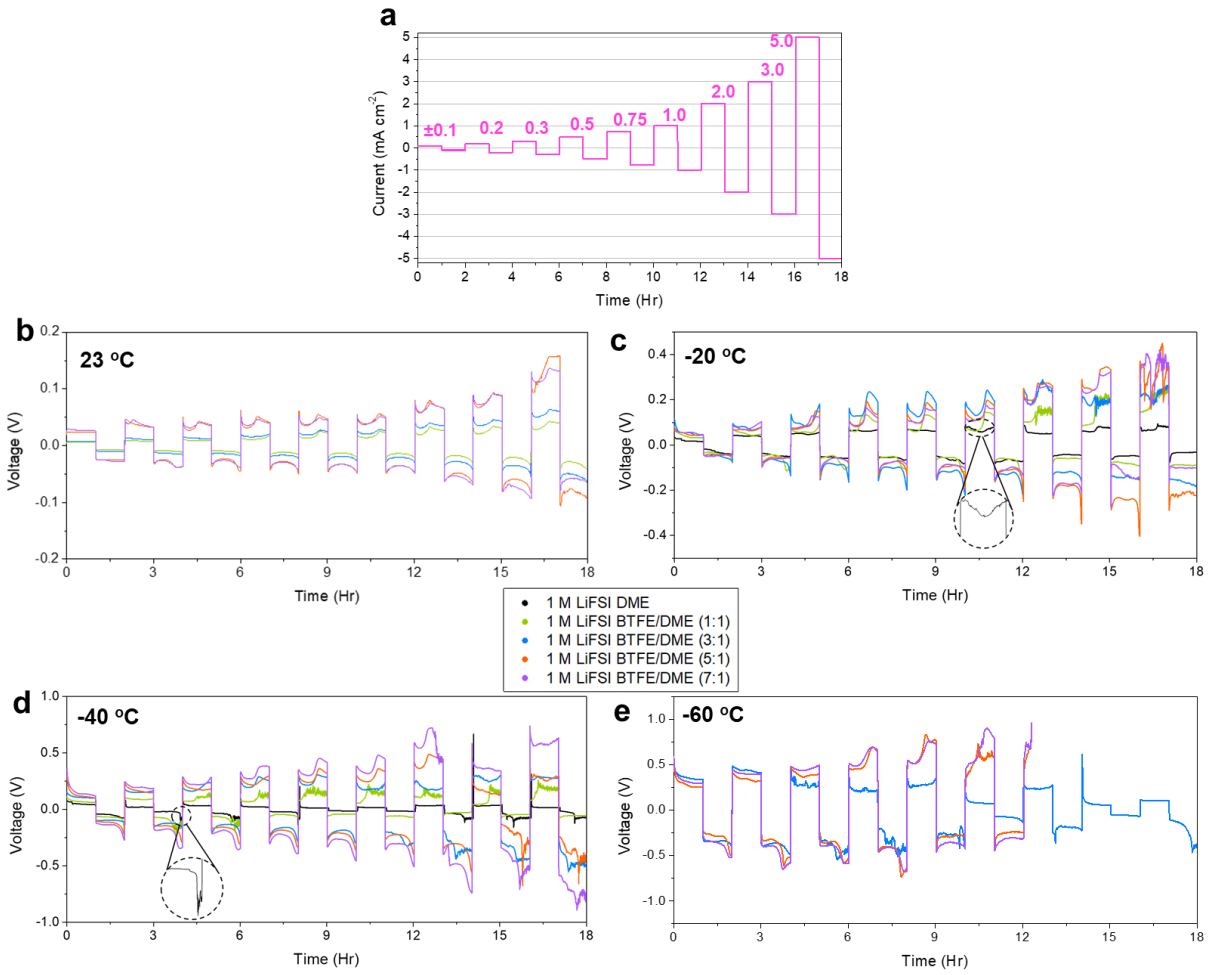

Figure S6. Critical current testing in Li||Li cells employing electrolytes of interest. **a)** Applied current scheme for all cells at all temperatures. Corresponding voltage profiles of electrolytes of interest at **b)** 23, **c)** -20, **d)** -40, and **e)** -60 °C. All cells were pre-cycled 2 times at room temperature at 0.5 mA cm^{-2} for 1 mAh cm^{-2} before testing.

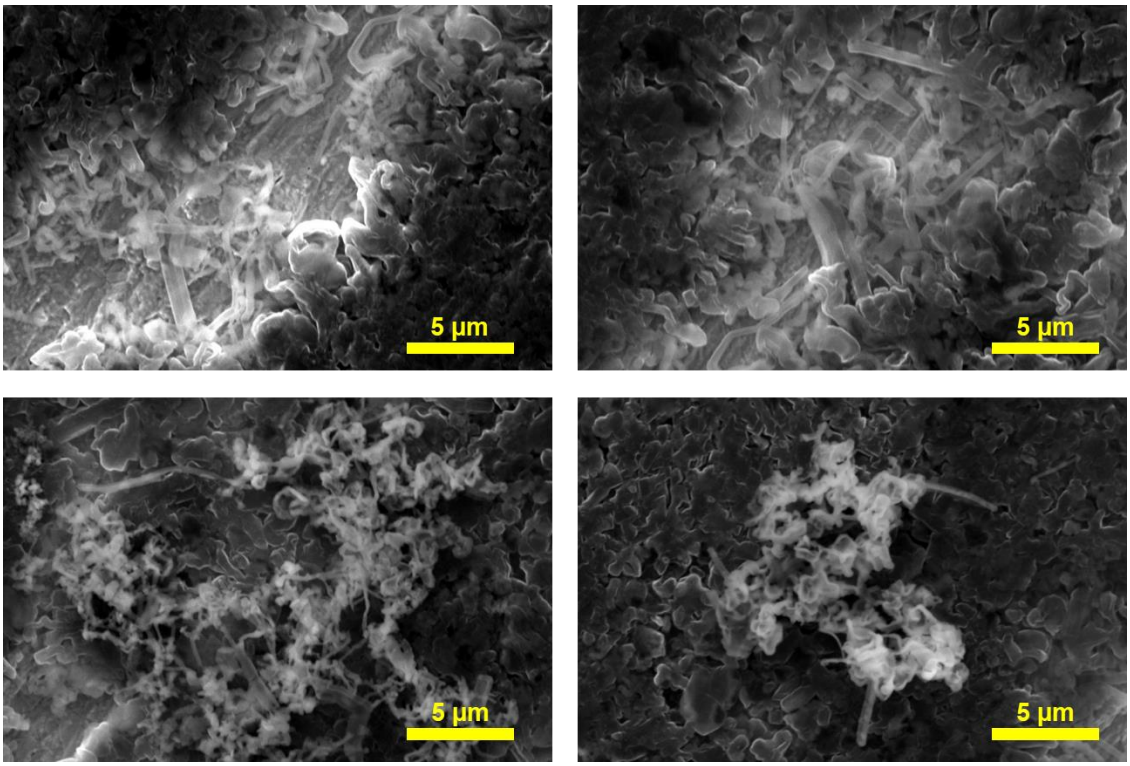

Figure S7. Additional SEM photographs of 5 mAh cm^{-2} of Li metal plated at 0.5 mA cm^{-2} and -40 ^{o}C in 1 M LiFSI DME.

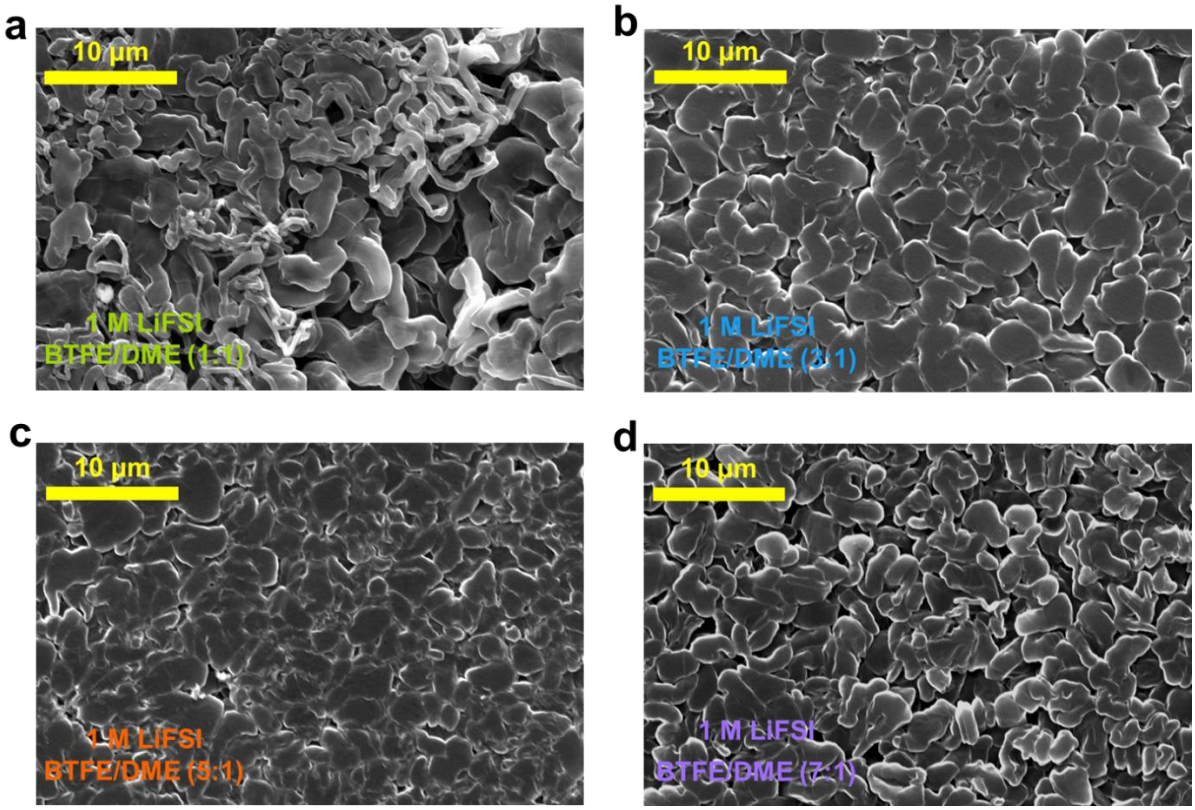

Figure S8. Planar SEM photographs of deposited Li metal at -20 °C in **a)** 1 M LiFSI BTFE/DME (1:1), **b)** 1 M LiFSI BTFE/DME (3:1), **c)** 1 M LiFSI BTFE/DME (5:1), **d)** 1 M LiFSI BTFE/DME (7:1).

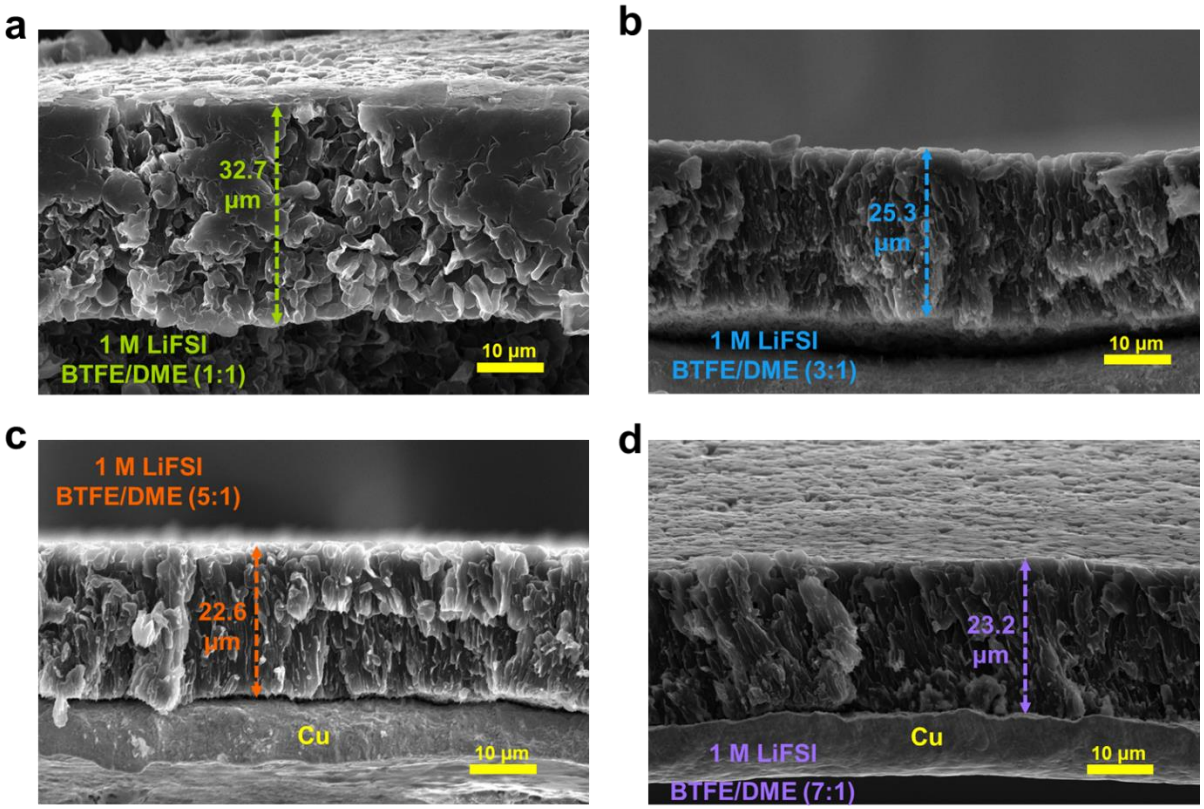

Figure S9. Cross-section SEM of 4 mAh cm^{-2} deposited Li metal at -20 ºC in **a)** 1 M LiFSI BTFE/DME (1:1), **b)** 1 M LiFSI BTFE/DME (3:1), **c)** 1 M LiFSI BTFE/DME (5:1), **d)** 1 M LiFSI BTFE/DME (7:1).

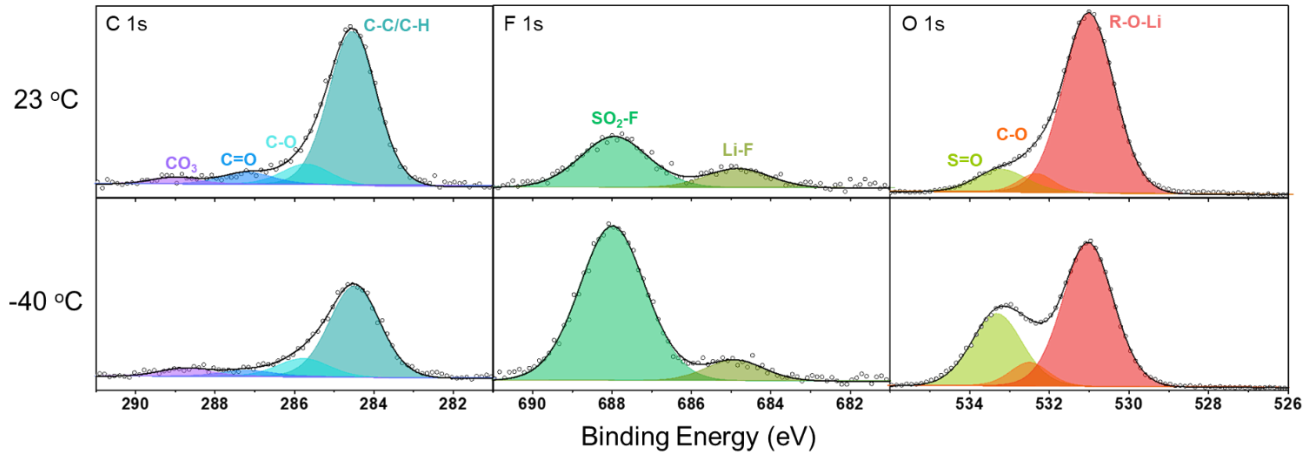

Figure S10. XPS spectra of Li metal after 1 deposition at 23 and -40 °C in 1 M LiFSI BTFE/DME (5:1).

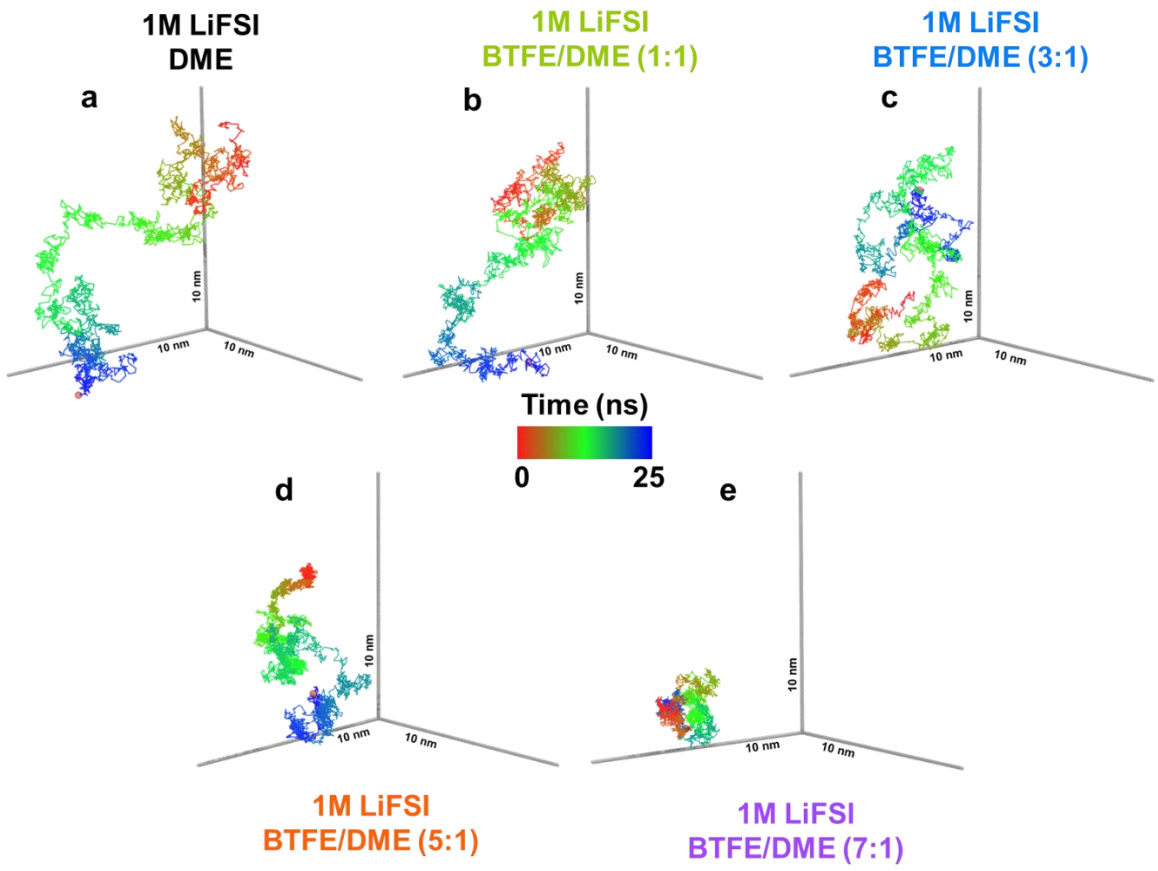

Figure S11. Visualized path of a Li^+ ion over the course of 25 ns from MD simulations of **a)** 1 M LiFSI DME, **b)** 1 M LiFSI BTFE/DME (1:1), **c)** 1 M LiFSI BTFE/DME (3:1), **d)** 1 M LiFSI BTFE/DME (5:1), **e)** 1 M LiFSI BTFE/DME (7:1).

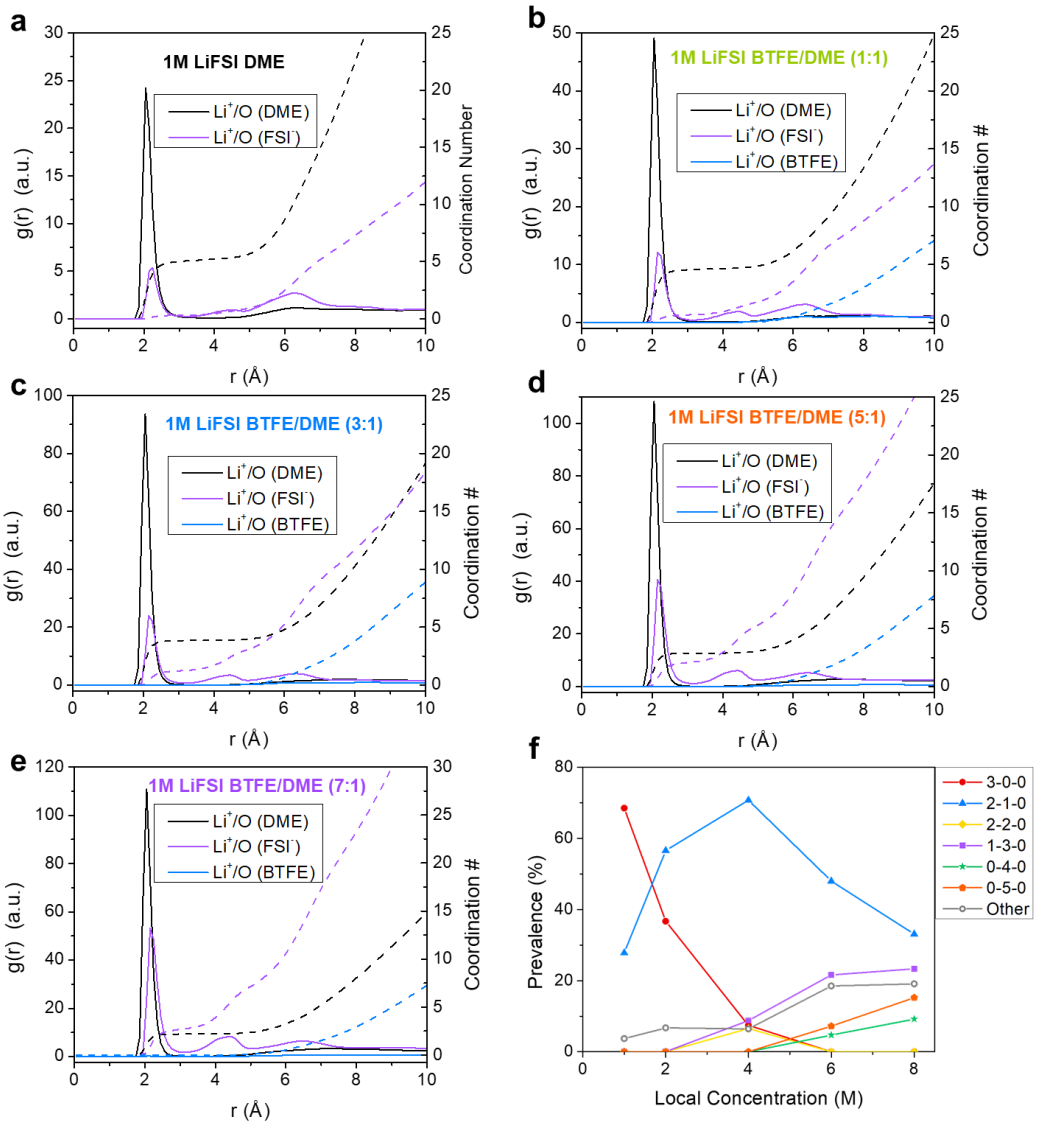

Figure S12. Radial distribution functions and coordination numbers of DME, FSI^- and BFTE oxygens with respect to Li^+ in **a)** 1 M LiFSI DME **b)** 1 M LiFSI BTFE/DME (1:1), **c)** 1 M LiFSI BTFE/DME (3:1), **d)** 1 M LiFSI BTFE/DME (5:1), and **e)** 1 M LiFSI BTFE/DME (7:1). **f)** Alternative representation of solvation species distribution with respect to local electrolyte concentration (e.g. 1 M LiFSI BTFE/DME 7:1 is considered an 8 M Local concentration).

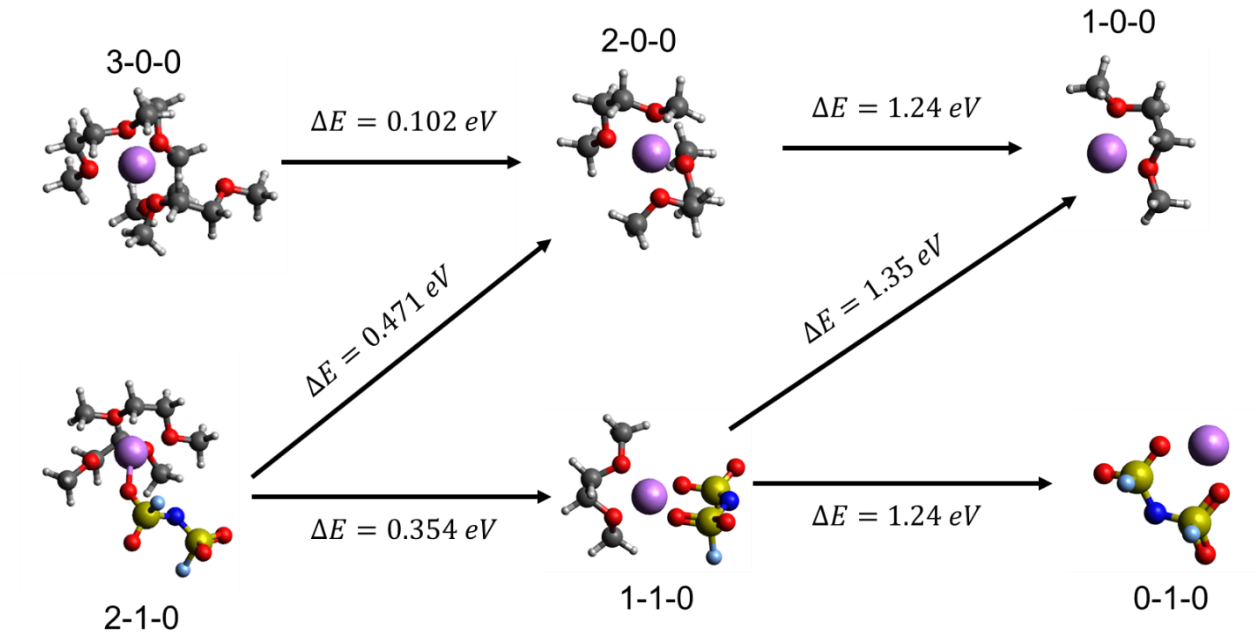

Figure S13. Molecular DFT energies associated with the removal of various components within the solvation shell. The "x-y-z" nomenclature was again adopted to portray solvation shells of $[Li(DME)_x(FSI)_y(BTFE)_z]^{1-y}$.

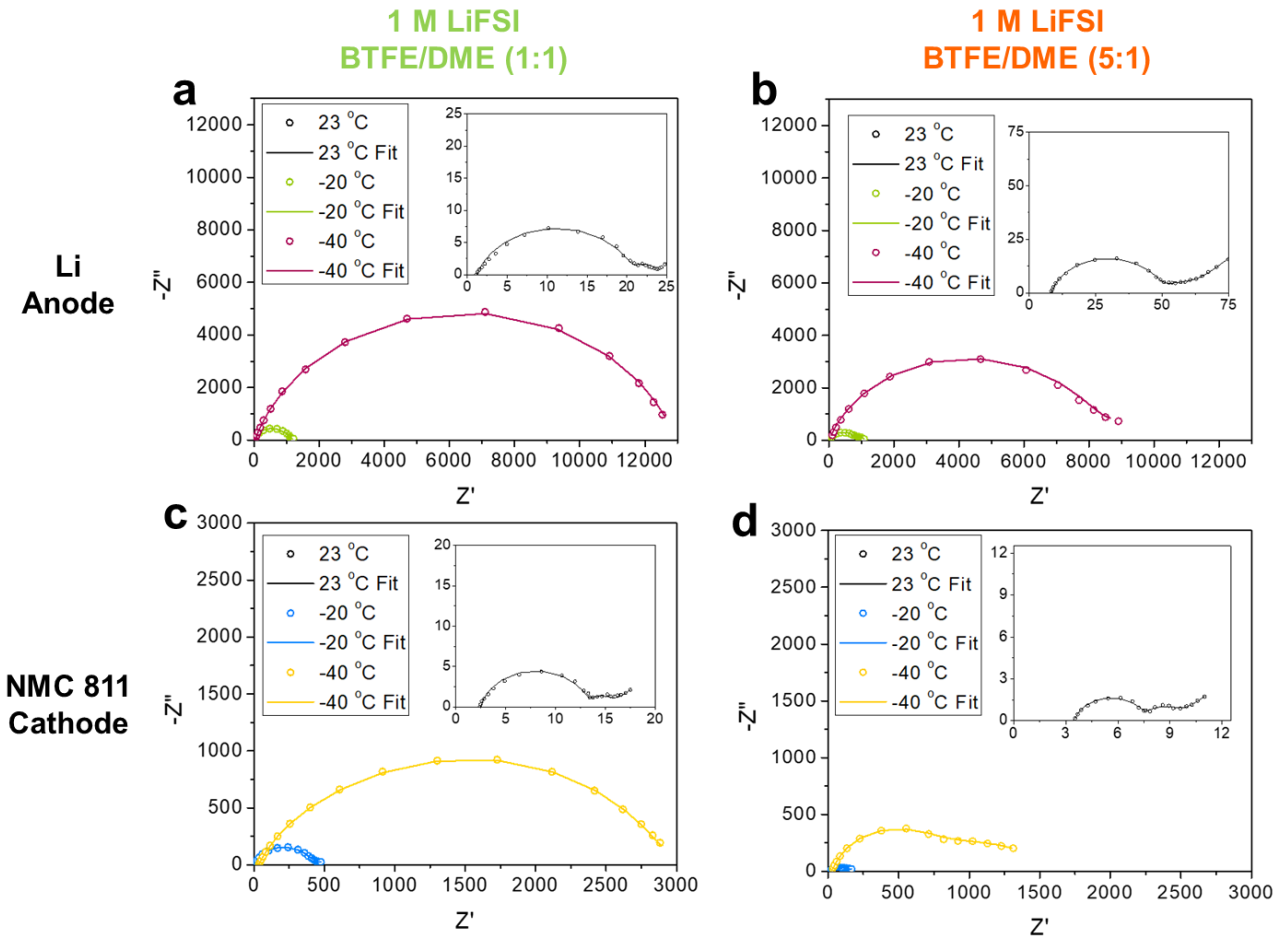

Figure S14. EIS spectra of 3 electrode coin cells as a function of temperature. Nyquist plots of Li metal anode in **a)** 1 M LiFSI BTFE/DME (1:1) and **b)** 1 M LiFSI BTFE/DME (5:1) Nyquist plots of NMC 811 cathode at 50 % in **c)** 1 M LiFSI BTFE/DME (1:1) and **d)** 1 M LiFSI BTFE/DME (5:1).

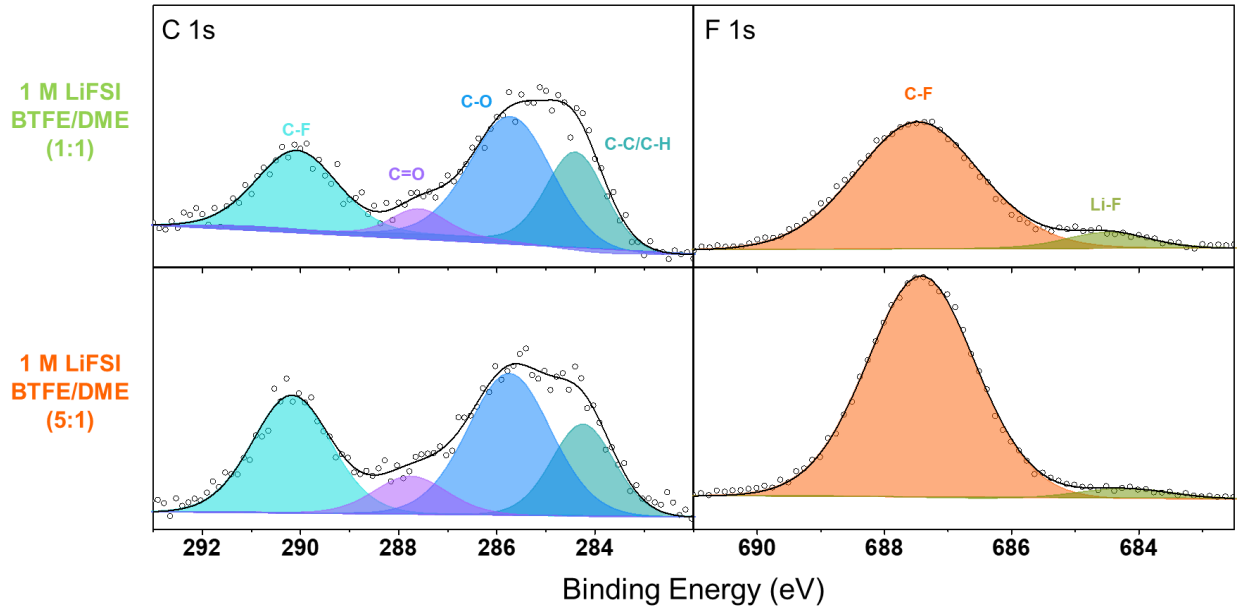

Figure S15. XPS spectra of NMC 811 after 10 cycles in 1 M LiFSI BTFE/DME (1:1) and 1 M LiFSI BTFE/DME (5:1).

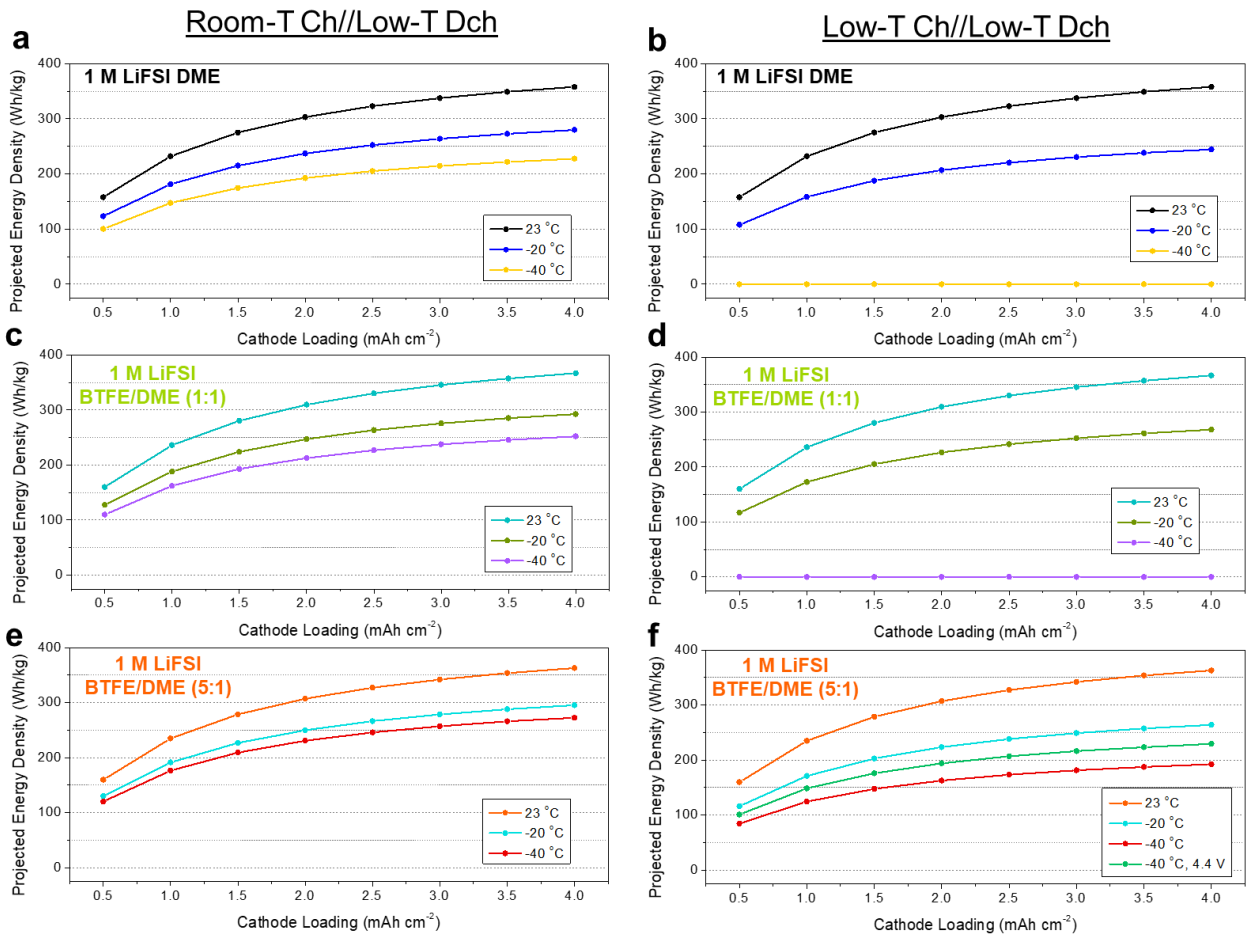

Figure S16. Cell-level energy density projections for pouch-type full cells with N/P = 2 and the parameters described in the methods section.

Table S2. Average voltage of NMC 811||Li full cells from energy density calculations

Electrolyte System	**23 ºC**	**-20 ºC**	**-40 ºC**
1 M LiFSI DME Room-T Charge, Low-T Discharge	3.82	3.74	3.62
1 M LiFSI BTFE/DME (1:1) Room-T Charge, Low-T Discharge	3.84	3.81	3.49
1 M LiFSI BTFE/DME (5:1) Room-T Charge, Low-T Discharge	3.86	3.80	3.68
1 M LiFSI DME Low-T Charge & Discharge	n/a	3.71	n/a, shorting
1 M LiFSI BTFE/DME (1:1) Low-T Charge & Discharge	n/a	3.77	n/a, shorting
1 M LiFSI BTFE/DME (5:1) Low-T Charge & Discharge	n/a	3.77	3.61 (4.3 V cutoff), 3.66 (4.4 V cutoff)

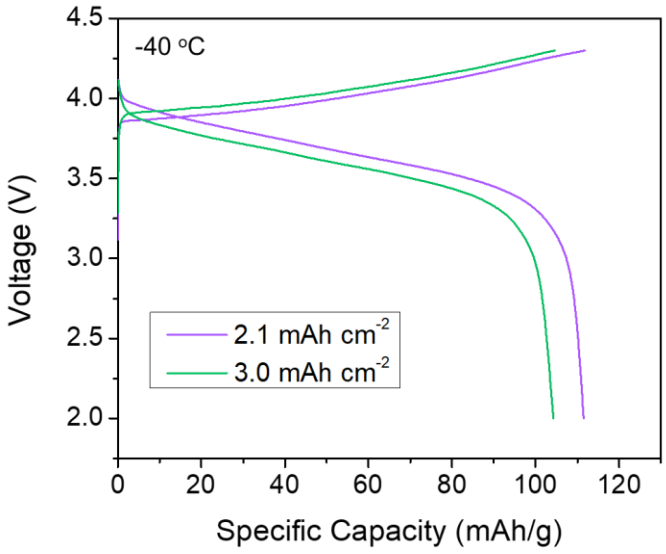

Figure S17. Voltage profiles of Li||NMC 811 full cells with altered cathode loading cycled at -40 ^{o}C and a 0.1 C rate.

References

[1] Ren, X.; Zou, L.; Cao, X.; Engelhard, M. H.; Liu, W.; Burton, S. D.; Lee, H.; Niu, C.; Matthews, B. E.; Zhu, Z.; Wang, C.; Arey, B. W.; Xiao, J.; Liu, J.; Zhang, J.-G.; Xu, W. Enabling High-Voltage Lithium-Metal Batteries under Practical Conditions. *Joule* **2019**, *3* (7), 1662–1676.

[2] He, M.; Hu, L.; Xue, Z.; Su, C. C.; Redfern, P.; Curtiss, L. A.; Polzin, B.; Cresce, A. von; Xu, K.; Zhang, Z. Fluorinated Electrolytes for 5-V Li-Ion Chemistry: Probing Voltage Stability of Electrolytes with Electrochemical Floating Test. *J. Electrochem. Soc.* **2015**, *162* (9), A1725.

[3] Adams, B. D.; Zheng, J.; Ren, X.; Xu, W.; Zhang, J.-G. Accurate Determination of Coulombic Efficiency for Lithium Metal Anodes and Lithium Metal Batteries. *Advanced Energy Materials 8* (7), 1702097.

[4] Kaminski, G. A.; Friesner, R. A.; Tirado-Rives, J.; Jorgensen, W. L. Evaluation and Reparametrization of the OPLS-AA Force Field for Proteins via Comparison with Accurate Quantum Chemical Calculations on Peptides. *J. Phys. Chem. B* **2001**, *105* (28), 6474–6487.

[5] L. Gouveia, A. S.; S. Bernardes, C. E.; C. Tomé, L.; I. Lozinskaya, E.; S. Vygodskii, Y.; S. Shaplov, A.; Canongia Lopes, J. N.; M. Marrucho, I. Ionic Liquids with Anions Based on Fluorosulfonyl Derivatives: From Asymmetrical Substitutions to a Consistent Force Field Model. *Physical Chemistry Chemical Physics* **2017**, *19* (43), 29617–29624.

[6] Park, C.; Kanduč, M.; Chudoba, R.; Ronneburg, A.; Risse, S.; Ballauff, M.; Dzubiella, J. Molecular Simulations of Electrolyte Structure and Dynamics in Lithium–Sulfur Battery Solvents. *Journal of Power Sources* **2018**, *373*, 70–78.

[7] W. Shinoda, M. Shiga, M. Mikami, Rapid estimation of elastic constants by molecular dynamics simulation under constant stress, Physical Review B 69 (2004) 134103.

[8] G.J. Martyna, D.J. Tobias, M.L. Klein, Constant pressure molecular dynamics algorithms, J. Chem. Phys. 101 (1994) 4177-4189.

[9] M. Parrinello, A. Rahman, Polymorphic transitions in single crystals: A new molecular dynamics method, J. Appl. Phys. 52 (1981) 7182-7190.

[10] M.E. Tuckerman, J. Alejandre, R. López-Rendón, A.L. Jochim, G.J. Martyna, A Liouville-operator derived measure-preserving integrator for molecular dynamics simulations in the isothermal–isobaric ensemble, J. Phys. A: Math. Gen. 39 (2006) 5629.

[11] Y. Shao, Z. Gan, E. Epifanovsky, A.T. Gilbert, M. Wormit, J. Kussmann, A.W. Lange, A. Behn, J. Deng, X. Feng, Advances in molecular quantum chemistry contained in the Q-Chem 4 program package, Mol Phys 113 (2015) 184-215.

[12] Betz, J.; Bieker, G.; Meister, P.; Placke, T.; Winter, M.; Schmuch, R. Theoretical versus Practical Energy: A Plea for More Transparency in the Energy Calculation of Different Rechargeable Battery Systems. *Advanced Energy Materials* **2019**, *9* (6), 1803170.

[13] Kwon, K.; Evans, J. W. Viscosity Changes of Li Battery Electrolytes and Their Long-Term Effect on the Frequency of EQCM Electrodes. *Electrochem. Solid-State Lett.* **2002**, *5* (3), A59.